# A tag-less ultrawide-band passive tracking system

Luca Santoro, Matteo Nardello, Davide Eccher, Mattia Sittoni, Davide Brunelli and Daniele Fontanelli
*Department of Industrial Engineering*, *University of Trento*, Trento, Italy
name.surname@unitn.it

***Abstract*—UltraWide-Band (UWB) low-power devices are becoming an increasingly effective solution for tracking and positioning systems, especially in IoT devices with limited power sources. Background models can be created by analysing the radio frequency or channel impulse response in a static environment. Comparing this background model with runtime measurements it is possible to identify moving objects inducing changes in the impulse responses, and as a consequence, we can compute the distance of the object from the radar devices, usually consisting of one transmitter and one receiver. In particular, using multiple receivers, it becomes possible to elaborate a 2D position of the moving object. This type of tag-less passive tracking system has the advantage of retrieving the trajectory of a moving object without the adoption of any additional electronic device. In this paper, we present an IoT positioning architecture achieving an RMSE of about 30 cm.**

***Index Terms*—UltraWide-Band, device-free localisation, sensor-less sensing, multipath-assisted localisation, passive localisation.**

## I. Introduction

Internet of Things (IoT) has quickly become pervasive in many application scenarios (e.g., as smart farming [1], [2], surveillance [3], [4], building automation [5], traffic telematics [6], structural health monitoring [7], environmental monitoring [8]) thanks to the increasing availability of compact and low-power devices used for data transmission and accurate sensing.

IoT uses many different Radio-Frequency (RF) technologies, like Wi-Fi, Bluetooth, 5G, or Ultrawide-Band (UWB), exploiting communication signals and their features at best. Moreover, techniques such as Received Strength Signal (RSS), Angle of Arrival (AoA), Phase of Arrival (PoA) or Time of Flight (ToF) are of primary importance for, e.g., obtaining spatial awareness about moving entities within an area. Several works are proposed in the literature for indoor/outdoor tracking and positioning systems based on such technologies. More in depth, we can classify localisation methods as *Device-Based* and *Device-Free*. The former assumes the entity to be tracked endowed with a device that participates actively in the localisation solution, while RF-based device-free localisation systems are tag-less, i.e., without the need of an electronic device mounted on the target. In [9], an indoor positioning system based on Bluetooth 5.1 and angle of arrival measurements is presented. [10] proposes a UWB infrastructure that utilises Time Difference of Arrival (TDoA) for tracking purposes. [11] adaptively builds a network of UWB anchors while exploring and unknown environments, while the study of the achievable accuracy is studied in details in [12]. The work in [13] uses a system based on Radio Signal Strength (RSS) to estimate the distance between one node and a target. Whereas, [14] introduces a UWB technology-based system that can track an unlimited number of receivers while maintaining the overall update rate and minimising the target uncertainty. In the context of a positioning system, [15] presents a discussion on a human-follower robot utilising ultrawide-band-vision data, while [16] proposes a leader-follower application for human-robot interaction based on UWB tracking.

Instead, the device-free approach is getting increasing attention as a solution in different application scenarios where we can not - or do not want to - equip the entity to be tracked with an electronic device. For example, as reported in [17], seniors' assistance or people with brain-related diseases assistance is the typical case in which the everyday duty of wearing, activating and recharging an electronic device may become a critical task. This is a typical case in which vision-based human activity monitoring comes handy, although it suffers several drawbacks, such as energy consumption, cost, and privacy concerns. In [18], a vision-based approach obtains excellent results at the cost of a reduced privacy level, not suitable in low-light conditions and high computational cost. In [19], an ultrasound positioning system is presented, which uses the echo signals to retrieve the distance between the emitter and the target, but it is prone to interference from other audio signals [20].

Apart from big radar systems developed at the beginning of the 20th century, low-power radio systems and human-centric services have revamped the research interests on device-free localisation, focusing on indoor and IoT applications. In this respect, a deep insight into IoT localisation methods could be found in [21]. Among the RF-based techniques, the most promising technology is the UltraWide-Band, due to its well-known characteristics of robustness to multipath [22] and to radio communication technologies. By means of an analysis on how the UWB radio frequency spectrum is affected by the moving entity and specifically addressing the Channel Impulse Response (CIR), it is possible to locate moving objects inside the propagation area. The CIR is a measure of the signal power at different time delays, and it is informative of the different paths a signal takes when traveling from a transmitter to a receiver. Hence, UWB radar systems can detect objects based on the trace spotted in the measured CIR. An interesting way to use the UWB sensor is in a radar-like system inspired by the *pulsed radar*. As described in [23], [24], when an entity is moving in an RF-flooded environment, the target's location can be detected thanks to the induced disturbance on the RF spectrum. This kind of localisation technique is referred to

as *multipath-assisted* localisation, based on detecting the RF scattering source leveraging the multipath components or the originally transmitted signal. In this case, the analysis of the RF spectrum of the static environment is needed to create the background model. Once a moving entity enters the scene, we can compare the background and RF spectrum to localise the entity by observing the CIR time variations.

This paper extends the preliminary evaluation done in [23] of an ultrawide-band bistatic radar in the following ways:

- We introduce a cost function to improve the estimates;
- We realised a distributed system to detect and track moving entities in the surrounding environment;
- We developed an IoT architecture to handle and sort the data using as much as possible the available bandwidth of the chosen UWB module;
- We enhance the processing update rate of the receiver, improving the maximum target velocity that the proposed system can track.

The rest of the paper is organised as follows. In Section II, we briefly present equations and mathematical models to infer from the CIR measurements the distance of the moving entity. Section III outlines the solutions we implemented to enhance the tracking system performance. Experimental results are discussed with the description of the IoT network and the prototype in Section IV. Section V concludes this work with final remarks, highlighting possible improvements and identifying new research problems.

## II. Background and Problem Formulation

This section provides a brief overview of the equations and models utilised position estimation of a mobile entity. However, for a more detailed understanding, we refer to our previous work that provides an in-depth reference on the topic [23].

Without compromising generality, we assume a scenario with three UWB transceivers consisting of one transmitter and two receivers deployed in a known area. We can describe each node by its known coordinates $P_i$, i.e.,

$$P = [P_1^{TX}, P_2^{RX}, P_3^{RX}] = \begin{bmatrix} x_1 & x_2 & x_3 \\ y_1 & y_2 & y_3 \end{bmatrix}. \tag{1}$$

By employing the UWB signal propagation model and sequentially gathering CIRs, we can extract the multipath components scattered from the target we intend to track. The Channel Impulse Response model, which includes deterministic multipath components with amplitude $a_i$ and delays $\tau_i$, and diffuse multipath components $\varepsilon(t)$ modelled as Additive Gaussian White Noise is reported next

$$h(t) = \sum_{i=1}^{l} a_i \delta(t - \tau_i) + \varepsilon(t), \tag{2}$$

where $l$ is the length of the CIR signal and where the autocorrelation of the uncertainty $\varepsilon(t)$ is given by

$$E(\varepsilon(t) * \varepsilon(t)) = S(t)\delta(t - \tau). \tag{3}$$

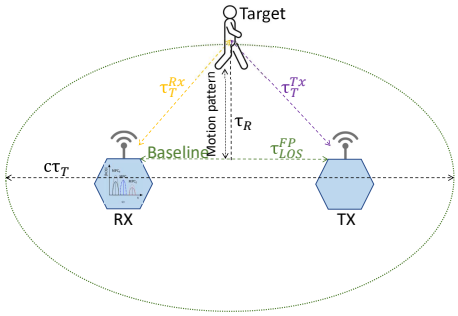


Figure 1. Bistatic radar configuration. $\tau_{LOS}^{FP}$ is the time of flight (ToF) in line-of-sight condition between receiver and transmitter, $\tau_T^{Rx}$ and $\tau_T^{Tx}$ is the ToF of the reflected signal between target and receiver and transmitter, respectively, $\tau_R$ the ToF with respect the centre of the bistatic radar and the target and $\tau_T$ is the major axis of the ellipse.

The tracked target can be considered as a virtual anchor with coordinates $P_T = [x_T, y_T]^T$ that transmits a delayed and attenuated version of the original signal emitted from the transmitter. The time of flight $t_i$ between the receiver $P_i^{RX}$ and the target for the $i$-th multipath component is given by

$$t_i = \frac{1}{c}\|P_i - T\|. \tag{4}$$

Considering a bistatic radar configuration as reported in Figure 1, the maximum distance at which the target is detectable can be calculated using the transmitted power peak and the sampling resolution of the receiver [25]. By imposing the following system of inequalities

$$\begin{cases} w = c\ l\ t_{ref}, \\ \frac{{\tau_{LOS}^{FP}}^2}{4} + \tau_R^2 = {\tau_T^{Rx}}^2, \\ \frac{{\tau_{LOS}^{FP}}^2}{4} + \tau_R^2 = {\tau_T^{Tx}}^2, \\ {\tau_T^{Tx}}^2 + {\tau_T^{Rx}}^2 \leq w, \end{cases} \tag{5}$$

we can compute the theoretical maximum distance for which the delayed signal falls inside the observation window permitted by the selected hardware, i.e., the hardware enables varying CIR lengths, which establishes the maximum duration of the observation window. In (5), the observation window is denoted by $w$, the speed of light by $c$, the length of the CIR by $l$, and the unit time for each CIR sample by $t_{ref}$. Additionally, we define $\tau_{LOS}^{FP}$ as the time-of-flight (ToF) in line-of-sight (LoS) between the transmitter and receiver, $\tau_R$ as the ToF between the target and the baseline of the bistatic radar, and $\tau_T^{Rx}$ and $\tau_T^{Tx}$ as the ToF between the target and the receiver and transmitter respectively.

The CIR signal should remain constant in a stable environment, but due to the instability of transmitters and receivers, a phase difference can occur between them. As a result, when a single receiver samples the CIR of a packet, the sampling point may differ from the previous sample. This sampling drift can be utilised to accumulate data and generate a more detailed structure of the CIR. In other words, by exploiting clock drift, we can obtain multiple samples, resulting in a wider sample rate compared to a single sampling operation. Once a series

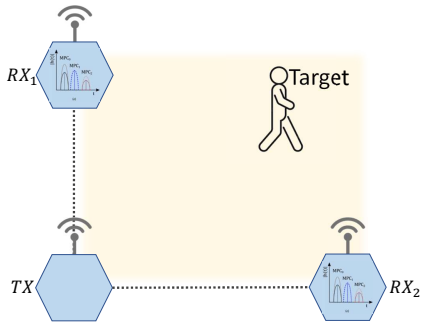


Figure 2. Representation of the detection area identified by anchors and transmitter.

of consecutive CIRs are obtained, they can be aligned based on the line-of-sight (LOS) peak time instant $\tau_{LOS}^{FP}$.

In a static environment, a TX-RX couple will consistently produce the same response to a known RF signal, resulting in the same Multipath Components (MPCs) being generated. As such, the model of the background response $h^B$ through the CIRs measurements can be obtained. A moving object into the environment results in new MPCs within the CIR associated with this entity. Computing the differences between the incoming and the background CIRs, the MPCs components coming from the moving entity can be determined. Considering each bistatic configuration of the system proposed in Figure 1, the target's position $P_T$, is subject to the constraint of lying on an ellipse. This ellipse has focal points located at $P_1^{TX}$ and $P_i^{RX}$, major axis equal to $c\ \tau_T$, and is described by

$$\|P_i^{RX} - P_T\| + \|P_1^{TX} - P_T\| = c\ \tau_T, \tag{6}$$

where $\tau_T$ is obtained using a variation of the algorithm described in [23], [24] . Once the location $P_T$ is determined, we implicitly obtain the ranging information. With two receivers, we can compute the target position within the convex area defined by the line-of-sight between each couple TX-RX as shown in Figure 2, with a maximum detecting range defined by (5).

### A. Position estimation

Once $\tau_T$ is obtained, different approaches could be used to estimate the coordinate of the target $\hat{P}_T = [\hat{x}_T, \hat{y}_T]^T$. For example, in [26] a method is presented that employs analytical techniques to determine the intersection points of multiple ellipses. In [27], an ellipse-resampling particle filter is developed for cooperative target tracking. This article does not focus on creating a complex estimation filter. Instead, we aim to enhance the precision of the raw data, which motivates the use of a particle filter. The particles' movements are modelled using a random walk, meaning that the position of each particle $p = [x_p, y_p]^T$ is assumed to change over time as

$$\begin{cases} x_p^{t+\Delta t} = x_p(t) + \Delta t \eta_{x_p}(t), \\ y_p^{t+\Delta t} = y_p(t) + \Delta t \eta_{y_p}(t). \end{cases} \tag{7}$$

At each prediction step, particle positions are updated with $\Delta t$, that is the elapsed time since the last measurement reception. The random variables $\eta_{x_p}(t)$ and $\eta_{y_p}(t)$ are a realisation of a stochastic process that follows a normal distribution with zero mean and standard deviation $\sigma_\eta$. Whenever an estimated $\hat{\tau}_T$ is received, the particles' weights are updated according to the marginalisation

$$w_p = p(\tau_T | \hat{\tau}_T), \tag{8}$$

where the expected $\tau_T$ is calculated using (6).

### B. Problem formulation and solution overview

Considering a multi-static radar as depicted in Figure 2 and given the CIRs measurements $h(t)$ in (2), we want to improve the $(\hat{\tau}_T^{RX_1}, \hat{\tau}_T^{RX_2})$ estimates. Besides, an IoT architecture capable of handling, sorting, and processing the CIRs measurements to estimate the target location $\hat{p}_T$ within the tracked area is required.

We have developed an IoT infrastructure using MQTT for realising data sharing between the UWB nodes and the processing unit. We have also introduced a new cost function to enhance the estimates of $\hat{\tau}_T$ and increased the update rate of the bistatic radar, thus making the infrastructure more flexible and user-friendly. Moreover, to prevent the bottleneck effect, we have implemented a message size reduction strategy to minimise the data transmitted within the IoT network.

## III. Solution

To estimate the target distance from each TX-RX couple, we need to build the RF response of the static environment by using consecutive CIR measurements $h$. Once the background model $h_B$ is computed, to highlight the foreground $h^F$, i.e., the moving objects, the following background subtraction technique is performed

$$h^F = h - \alpha h_B, \tag{9}$$

where $\alpha \in (1, 2]$ is a constant value that scales the background signal to avoid ripples for very small values after applying (9). To improve the precision of the estimate of $\hat{\tau}_T$, we introduce a cost function to weight each single values of the signal $h^F$, i.e.

$$\text{cost} = W(h_i^F, h_j^F) \frac{h_i^F}{h_{max}^F} \frac{h_{peak}^F}{h_{max}^F}, \tag{10}$$

where $W(h_i^F, h_j^F)$ is the observation window, whose length is defined by the number of elements in $\{i, \ldots, \min\{j \in \mathbb{N} | h_j^F \leq h_i^f \wedge j \geq i\} - 1\}$, $h_{peak}^F$ is the value of the the first peak within $W(h_i^F, h_j^F)$, $h_i^F$ is the $i$-th sample of the resulting signal $h^F$, and $h_{max}^F$ the maximum value of the entire CIR.

The cost function in (10) emphasises the significance of several factors that affects the estimate of $\hat{\tau}_T$. One such factor is the window dimension, since it should be large enough to ensure that the detected target has produced multiple MPCs that were not present in the background model. The starting value $h_i$ of the window is also essential, as a higher value suggests that the target detection is more significant. Finally,

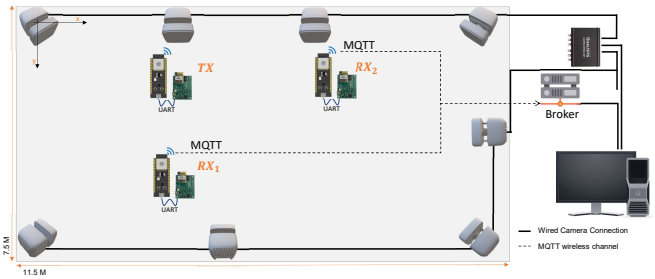


Figure 3. Experimental setup

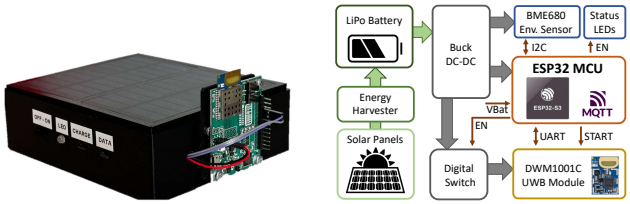


(a) (b)

Figure 4. In (a) the developed prototype, in (b) the HW architecture.

the first peak value is critical since it indicates the direct multipath generated when an object enters the scene. This value should be sufficiently high to ensure that the starting point of the window coincides precisely with the direct multipath time location $\hat{\tau}_T$. To avoid erroneous timestamps transmitted by the receivers, caused by the influence of ambient noise that may lead to a faulty reading of the complex values to reconstruct the CIR, the incoming signals are filtered by a Gaussian filter. At this stage, we can multiply the value of $\hat{\tau}_T$ by the speed of light $c$ to obtain the estimated distance between the $i$-th radar baseline and the target. Once at least two measurements $\hat{\tau}_T$ are collected, we can use the particle filter to estimate the target position.

Sensor data is gathered and transmitted to a Raspberry Pi via the UART interface, which enables string-based data transfer. As a result, all important sensor data must be serialised to obtain a string of data representing the incoming information in ASCII format. To optimise the performance in real-time applications, we strive to keep the size of the transmitted data as small as possible.

After decoding all the data, they need to be sent to the central computing unit for processing and extracting the location of the tracked object. To achieve this, we utilise MQTT middleware, which operates on a publish/subscribe protocol. The overall architecture is reported for reference in Figure 3.

## IV. Experimental Results

We performed multiple tests to evaluate the proposed architecture and the effectiveness of the cost function. Initially, we concentrated on a single couple TX-RX, to assess the effectiveness of the previously depicted estimation process of $\tau_T$. This first phase is also helpful to highlight the issues related to the reconstruction using sequential CIR measurements and the leading edge detection algorithm

### A. Hardware

We have developed an UWB radar node, as shown in Figure 4, to implement the proposed IoT architecture. The UWB radio module is built around the Qorvo DWM1001 transceiver, compliant with the IEEE 802.15.4-2011 standard [28]. It can operate on six different frequency bands with centre frequencies ranging from 3.5 to 6.5 GHz and bandwidths of either 500 or 900 MHz. The chip can measure range and retrieve the measured CIR, and it offers three different data rates: 110 kbps, 850 kbps, and 6.8 Mbps. The DW1000 timestamps transmitted and received frames with a precision of 40 bits, using a nominal 64 GHz resolution. This results in a timing precision of 15.65 ps for packet timestamps. The UWB module is connected to an Espressif ESP32 microcontroller through the UART port. This microcontroller is powered by the Xtensa dual-core 32 bit LX6 microprocessor with a clock speed of up to 240 MHz. It also features WI-FI and Bluetooth modules enabling seamless wireless network integration. The microcontroller is also optimised for low power consumption, making it well-suited for wireless IoT applications. In order to facilitate tracking in areas without access to electricity, we have incorporated two solar panels to power the radar node. We track the experimental area using both the radar system and a motion capture system, which provides the ground truth to evaluate the accuracy of the proposed system. For the following experiments, we used a motion capture system provided by Qualisys with 8 Arqus A9 cameras, a synchronisation unit, and a dedicated workstation (see Figure 3).

One crucial factor to consider in the setup is the placement of the sensors within the environment. It is imperative to position the receivers at a distance from each wall in the room that is not similar to the distance estimated for the tracked entity. Otherwise, the wall could cause a peak in CIRs, leading to a false detection by the leading edge detection algorithm. In order to address this issue, it may be advisable to relocate the transceiver nearer to the wall. However, in our particular experimental configuration, this course of action is not feasible due to the physical limitations imposed by the furniture and the requirement to connect the receivers to a USB cable for the purpose of downloading supplementary data that is crucial to validate the proposed system.

### B. Results

Initially, a single couple TX-RX is used to evaluate the proposed method's effectiveness in distance calculation. In Figure 5-(a) is shown the results of the experiment conducted while performing a backward-forth movement with a varying motion speed ranging from 0.5 m/s to 1.5 m/s. As highlighted in Figure 5-(a) and described in the previous work [23], regions that are closer or farther away from the bistatic radar exhibit greater errors in the distance estimation. In Figure 5-(b) is reported the histogram of the experiment, with a mean error $\mu = 101$ mm and a standard deviation $\sigma = 195$ mm.

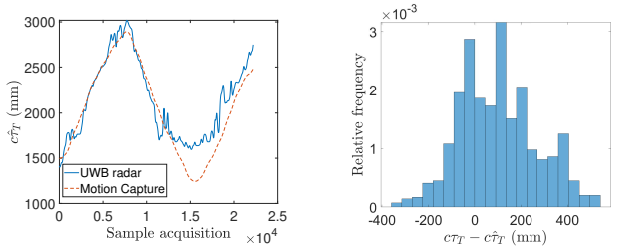


(a) (b)

Figure 5. In (a) comparison between the distance estimated by our approach (blue line) and distance retrieved by the motion capture (dashed-orange line), in (b) the histogram of the error.

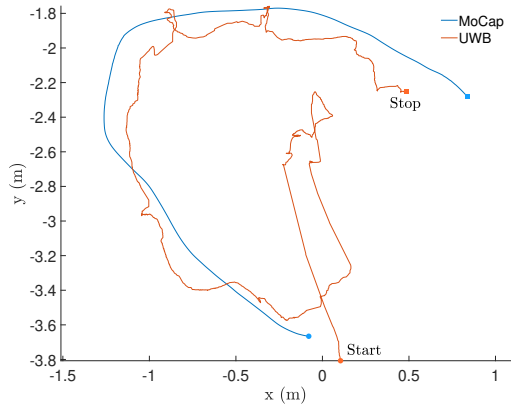


Figure 6. Comparison between target path estimated by UWB and by the MoCap.

It is worthwhile to note that the sampling rate of the receivers is fundamental. In our previous work [23], we limit the target velocity to be lower than 0.15 m/s to account for the system sampling rate and increase the tracking precision. Indeed, the bottleneck of the previous architecture was related to the bandwidth of the UART interface. Due to this constraint, we take care of the data encoding and, after the fine-tuning the algorithm, the system can now process and transmit data via MQTT at a frequency of 115 Hz, which is four times the previous work, that was capable of operating at 30 Hz rate.

Finally, Figure 6 shows the result of one tracking experiment. After the initial stage of convergence, the estimated position has an RMSE($\hat{P}_T$) of approximately 30 centimetres.

## V. Conclusion

Device-Free localisation offers many opportunities for various security, logistics, or IoT services applications. In this paper, we have further investigated the leading edge algorithm and introduced a cost function to refine the estimate of $\hat{\tau}_T$. We have also established a comprehensive IoT network and created a self-powered UWB radar node. We have also addressed the data size issue and improved the receiver unit's processing capacity from 30 Hz to 110 Hz. By implementing these measures, we have been able to increase the tracking speed of the low-cost UWB chip-based radar system from 0.15 m/s to 1.5 m/s. A particle filter has enabled us to achieve an RMSE($\hat{P}_T$) of approximately 30 cm.

The potential of the presented work paves the way for several extensions as future works. We will expand the number of receivers within the network to enhance the accuracy of estimated positions for moving entities. We will also improve multi-target tracking methods for scaling up to tens of entities.

## Acknowledgments

This research received funds by Fondazione VRT - Fondazione per la Valorizzazione della Ricerca Trentina.

## References

[1] G. Rajesh, B. Saroja, A. Gurulakshmi, and R. S. Malladi, "Enhanced time-to-time monitoring and surveillance in agriculture warehouse for diverse harvest crop yields through iot gadget," in *2022 International Conference on Distributed Computing, VLSI, Electrical Circuits and Robotics ( DISCOVER)*, 2022, pp. 172–175.

[2] A. Albanese, M. Nardello, and D. Brunelli, "Automated pest detection with dnn on the edge for precision agriculture," *IEEE Journal on Emerging and Selected Topics in Circuits and Systems*, vol. 11, no. 3, pp. 458–467, 2021.

[3] P. M. Jacob, J. Moni, A. Aji, Rashida, D. M. John, and G. G. Pillai, "An automated intrusion detection system with audio alert using passive infrared sensor," in *2022 International Conference on Data Analytics for Business and Industry (ICDABI)*, 2022, pp. 109–113.

[4] M. Nardello, H. Desai, D. Brunelli, and B. Lucia, "Camaroptera: A batteryless long-range remote visual sensing system," in *Proceedings of the 7th International Workshop on Energy Harvesting and Energy-Neutral Sensing Systems*. New York, NY, USA: Association for Computing Machinery, 2019, p. 8–14.

[5] D. Brunelli, I. Minakov, R. Passerone, and M. Rossi, "Povomon: An ad-hoc wireless sensor network for indoor environmental monitoring," in *2014 IEEE Workshop on Environmental, Energy, and Structural Monitoring Systems Proceedings*, 2014, pp. 1–6.

[6] L. F. Herrera-Quintero, K. Banse, J. Vega-Alfonso, and A. Venegas-Sanchez, "Smart its sensor for the transportation planning using the iot and bigdata approaches to produce its cloud services," in *2016 8th Euro American Conference on Telematics and Information Systems (EATIS)*, 2016, pp. 1–7.

[7] F. Di Nuzzo, D. Brunelli, T. Polonelli, and L. Benini, "Structural health monitoring system with narrowband iot and mems sensors," *IEEE Sensors Journal*, vol. 21, no. 14, pp. 16 371–16 380, 2021.

[8] P. Tosato, D. Facinelli, M. Prada, L. Gemma, M. Rossi, and D. Brunelli, "An autonomous swarm of drones for industrial gas sensing applications," in *2019 IEEE 20th International Symposium on "A World of Wireless, Mobile and Multimedia Networks" (WoWMoM)*, 2019, pp. 1–6.

[9] G. Maus, H. Pörner, R. Ahrens, and D. Brückmann, "A phase normalization scheme for angle of arrival based bluetooth indoor localization," in *2022 IEEE 65th International Midwest Symposium on Circuits and Systems (MWSCAS)*, 2022, pp. 1–5.

[10] J. Leng, G. Ma, J. Zhu, and H. Ma, "Improved tdoa two-stage uwb localization algorithm for indoor mobile robot," in *2021 IEEE International Conference on Recent Advances in Systems Science and Engineering (RASSE)*, 2021, pp. 1–5.

[11] L. Santoro, D. Brunelli, and D. Fontanelli, "On-line Optimal Ranging Sensor Deployment for Robotic Exploration," *IEEE Sensors Journal*, vol. 22, no. 6, March 2022.

[12] D. Fontanelli, F. Shamsfakhr, and L. Palopoli, "Cramer-Rao Lower Bound Attainment in Range-only Positioning using Geometry: The G-WLS," *IEEE Trans. on Instrumentation and Measurement*, vol. 70, pp. 1–14, October 2021.

[13] Z. Luo and B. Li, "Contributions of reference units to final result in indoor positioning system based on rss," in *2016 IEEE Information Technology, Networking, Electronic and Automation Control Conference*, 2016, pp. 186–189.

[14] L. Santoro, M. Nardello, D. Brunelli, and D. Fontanelli, "Scale up to infinity: the uwb indoor global positioning system," in *2021 IEEE International Symposium on Robotic and Sensors Environments (ROSE) Proceedings*. Piscataway, NJ, USA: IEEE, 2021, pp. 1–8.

[15] A. Luchetti, A. Carollo, L. Santoro, M. Nardello, D. Brunelli, P. Bosetti, and M. De Cecco, "Human identification and tracking using ultra-wideband-vision data fusion in unstructured environments," *ACTA IMEKO*, vol. 10, pp. 124–131, 2021.

[16] L. Santoro, M. Nardello, M. Calliari, W. C. Guarienti, G. Luchi, D. Fontanelli, and D. Brunelli, "Catch-me-if-you-can infrastructure-less uwb-based leader-follower system for compact uavs," in *2022 IEEE International Symposium on Robotic and Sensors Environments (ROSE)*, 2022, pp. 1–7.

[17] S. Shukri, L. M. Kamarudin, and M. H. F. Rahiman, "Device-free localization for human activity monitoring," in *Intelligent Video Surveillance*, A. J. R. Neves, Ed. Rijeka: IntechOpen, 2018, ch. 6. [Online]. Available: https://doi.org/10.5772/intechopen.79442

[18] E. M. Gorostiza, M. Á. G. Garrido, D. Pizarro-Perez, D. Salido, and P. Torres, "An indoor positioning approach based on fusion of cameras and infrared sensors," *Sensors (Basel, Switzerland)*, vol. 19, 2019.

[19] A. Kitanov, V. Tubin, and I. Petrovic, "Extending functionality of rf ultrasound positioning system with dead-reckoning to accurately determine mobile robot's orientation," in *2009 IEEE Control Applications, (CCA) & Intelligent Control, (ISIC)*, 2009, pp. 1152–1157.

[20] L. Li, R. Bai, B. Xie, Y. Peng, A. Wang, W. Wang, B. Jiang, J. Liang, and X. Chen, "R&p: An low-cost device-free activity recognition for e-health," *IEEE Access*, vol. 6, pp. 81–90, 2018.

[21] P. S. Farahsari, A. Farahzadi, J. Rezazadeh, and A. Bagheri, "A survey on indoor positioning systems for iot-based applications," *IEEE Internet of Things Journal*, vol. 9, no. 10, pp. 7680–7699, 2022.

[22] S. Geng, S. Ranvier, X. Zhao, J. Kivinen, and P. Vainikainen, "Multipath propagation characterization of ultra-wide band indoor radio channels," in *2005 IEEE International Conference on Ultra-Wideband*, 2005, pp. 11–15.

[23] M. Doglioni, L. Santoro, M. Nardello, D. Fontanelli, and D. Brunelli, "Cost-effective bistatic radar with ultrawide-band radio," in *2022 IEEE International Workshop on Metrology for Industry 4.0 and IoT (MetroInd4.0andIoT)*, 2022, pp. 207–211.

[24] A. Ledergerber and R. D'Andrea, "A multi-static radar network with ultra-wideband radio-equipped devices," *Sensors*, vol. 20, p. 1599, 03 2020.

[25] E. Paolini, A. Giorgetti, M. Chiani, R. Minutolo, and M. Montanari, "Localization capability of cooperative anti-intruder radar systems," *EURASIP Journal on Advances in Signal Processing*, vol. 2008, no. 1, p. 726854, Apr 2008.

[26] D. Kocur, M. Švecová, and J. Rovňáková, "Through-the-wall localization of a moving target by two independent ultra wideband (uwb) radar systems," *Sensors*, vol. 13, no. 9, pp. 11 969–11 997, 2013.

[27] C. Xu, X. Wang, S. Duan, and J. Wan, "Spatial-temporal constrained particle filter for cooperative target tracking," *Journal of network and computer applications*, vol. 176, p. 102913, 2021.

[28] I. . W. Group *et al.*, "Ieee standard for local and metropolitan area networks—part 15.4: Low-rate wireless personal area networks (lr-wpans)," *IEEE Std*, vol. 802, pp. 4–2011, 2011.